



Article

Vulnerability of Wetlands Due to Projected Sea-Level Rise in the Coastal Plains of the South and Southeast United States

Luis Lizcano-Sandoval ^{1,2,*}, James Gibeaut ³, Matthew J. McCarthy ⁴, Tylar Murray ¹, Digna Rueda-Roa ¹

- Institute for Marine Remote Sensing, College of Marine Science, University of South Florida, St. Petersburg, FL 33701, USA; tylarmurray@usf.edu (T.M.); druedaro@usf.edu (D.R.-R.); carib@usf.edu (F.E.M.-K.)
- ² Environmental Mapping, Spatial Informatics Group, Pleasanton, CA 94566, USA
- ³ Harte Research Institute for Gulf of Mexico Studies, Texas A&M University—Corpus Christi, Corpus Christi, TX 78412, USA; james.gibeaut@tamucc.edu
- Remote Sensing Group, Geospatial Science and Human Security Division, Oak Ridge National Laboratory, Oak Ridge, TN 37830, USA; mccarthymj@ornl.gov
- * Correspondence: luislizcanos@usf.edu

Abstract: Coastal wetlands are vulnerable to accelerated sea-level rise, yet knowledge about their extent and distribution is often limited. We developed a land cover classification of wetlands in the coastal plains of the southern United States along the Gulf of Mexico (Texas, Louisiana, Mississippi, Alabama, and Florida) using 6161 very-high (2 m per pixel) resolution WorldView-2 and WorldView-3 satellite images from 2012 to 2015. Area extent estimations were obtained for the following vegetated classes: marsh, scrub, grass, forested upland, and forested wetland, located in elevation brackets between 0 and 10 m above sea level at 0.1 m intervals. Sea-level trends were estimated for each coastal state using tide gauge data collected over the period 1983–2021 and projected for 2100 using the trend estimated over that period. These trends were considered conservative, as sea level rise in the region accelerated between 2010 and 2021. Estimated losses in vegetation area due to sea level rise by 2100 are projected to be at least 12,587 km², of which 3224 km² would be coastal wetlands. Louisiana is expected to suffer the largest losses in vegetation (80%) and coastal wetlands (75%) by 2100. Such high-resolution coastal mapping products help to guide adaptation plans in the region, including planning for wetland conservation and coastal development.

Keywords: high-resolution satellite images; coastal wetlands; sea-level rise; land cover classification; digital elevation model; airborne lidar



Citation: Lizcano-Sandoval, L.;
Gibeaut, J.; McCarthy, M.J.; Murray, T.;
Rueda-Roa, D.; Muller-Karger, F.E.
Vulnerability of Wetlands Due to
Projected Sea-Level Rise in the Coastal
Plains of the South and Southeast
United States. *Remote Sens.* 2024, 16,
2052. https://doi.org/10.3390/
rs16122052

Academic Editors: Dehua Mao, Chao Chen, Dong Li, Xiyong Hou and Weiwei Sun

Received: 13 April 2024 Revised: 28 May 2024 Accepted: 4 June 2024 Published: 7 June 2024



Copyright: © 2024 by the authors. Licensee MDPI, Basel, Switzerland. This article is an open access article distributed under the terms and conditions of the Creative Commons Attribution (CC BY) license (https://creativecommons.org/licenses/by/4.0/).

1. Introduction

Coastal wetlands are areas permanently or temporarily inundated by marine water. These areas provide habitat for terrestrial, aerial, and aquatic organisms [1]. They can mitigate the impacts of coastal storms and erosion [2,3] and store large quantities organic carbon [4,5]. The ecosystem services of coastal wetlands are considered essential [6].

Wetlands of the Atlantic and Gulf of Mexico coastal plain of the United States are a mixture of marshes, wet meadows, swamps including mangroves, and wet flatwoods [7]. Surface area estimates of these coastal wetland areas are difficult to find in part because of differences in how wetlands are defined and delimited, seasonal cover changes, and mapping quality [8,9].

Today, wetland mapping and monitoring is typically carried out using aerial and satellite remote sensing [10–12]. Land cover mapping in the United States is routinely done by the U.S. Fish and Wildlife Service (FWS), U.S. Geological Survey (USGS), and partners like the National Oceanic and Atmospheric Administration (NOAA), the U.S. Environmental Protection Agency (EPA), and various state agencies and research institutions.

Remote Sens. **2024**, 16, 2052 2 of 17

The federal efforts produce the National Wetland Inventory (NWI) and the National Land Cover Database (NLCD), which are updated every three to five years, respectively [13,14]. The Coastal-Change Analysis Program (C-CAP) from NOAA is the coastal expression of the NLCD. The NWI is produced from high-altitude airborne imagery, while the NLCD is derived using Landsat imagery at a nominal 30 m spatial resolution per pixel. Wetland mapping at higher spatial resolution is more accurate than coarser resolution products. For example, McCarthy et al. [11] classified wetlands in West Florida with WorldView-2 imagery at 2 m per pixel resolution and found higher accuracy in identifying forested wetland and upland vegetation compared to the NWI and C-CAP products. As more commercial satellite data become available, all agencies have started to develop land cover maps at spatial resolution finer than 10–30 m per pixel.

Major factors that are affecting wetland degradation and loss include human development (e.g., pollution, urban and other infrastructure, agriculture) and climate change [15–17]. In the United States, wetland areas decreased approximately 50% between 1780 and 2009. Nearly 50–60% of that loss was due to urban development and agriculture [8]. An important factor in planning for wetland conservation is sea-level rise (SLR). It has been estimated that 68% of coastal wetlands in 86 developing countries will be at risk if sea level were to rise 1 m [18]. Schuerch et al. [19] estimated global wetland losses between 0% and 30% by 2100 due to SLR alone. Osland et al. [20] estimated that in the United States, the highest potential for wetland loss by 2100 is in the states of Louisiana (29%), Florida (25%), North Carolina (10%), Texas (8%), and South Carolina (7%), considering a 1.5 m SLR scenario by 2100. Reed et al. [21] modeled three different scenarios of SLR for Louisiana in a 50-year period between 2015 and 2064 using a digital elevation model (DEM) at 30 m resolution. They estimated land losses, including wetlands, of between 3000 km² and 10,000 km² by 2064.

In this study, we refine the estimates of potential coastal wetlands losses in the south and southeast US using land cover maps and digital elevation models at much higher spatial resolution than the 30 m grid size previously available. This work is divided into three subsections: (1) development of a land cover map at high resolution (2 m pixels) of the coastal south and southeast United States; (2) estimation of areas of vegetation and wetland cover, including the distribution of wetland types in specific topographic bins; and (3) projected vegetation and wetland area loss given mean local SLR trends.

2. Materials and Methods

2.1. Study Area

This study focused on the coastal areas of the south and southeast United States (Texas, Louisiana, Mississippi, Alabama, and Florida) (Figure 1). All data products described below are accessible via the 3D-Wetlands app in Google Earth Engine (GEE), https://lizcanosandoval.users.earthengine.app/view/hr-land-cover-gulf-of-mexico, or the GitHub repository, https://github.com/luislizcano/3D-wetlands-app (accessed on 3 June 2024).

2.2. Satellite Data Processing

A total of 10,245 multispectral images spanning 2009 to 2018 collected with the WorldView-2 (8689) and World-View-3 (1556) satellites were obtained from the Digital-Globe (Maxar) repository and screened for cloud cover. The WorldView-2 satellite sensor, launched in October 2009, provided data in eight spectral bands at ~2 m per pixel (Table 1). WorldView-3 was launched in August 2014, provided imagery in similar bands as WorldView-2, but from a lower orbit and at ~1.5 m per pixel. We only used WorldView-3 data in bands that matched those of WorldView-2 and did not use the eight short-wave infrared bands. We focused on the period 2012 to 2015 to derive land cover and used those maps to estimate coastal wetland losses due to future SLR. This period was when the largest number of images was available to cover the whole region (Figure 1A,B). Specifically, we used 6161 images with cloud coverage less than 20%, distributed as follows: 2012 (1622 images), 2013 (1185 images), 2014 (2364 images), and 2015 (990 images). Most of the

Remote Sens. 2024, 16, 2052 3 of 17

satellite imagery corresponds to WorldView-2 with 5185 images. WorldView-3 provided 976 images. Data were mapped and reprojected to a spatial resolution of 2 m per pixel as described in McCarthy et al. [11].

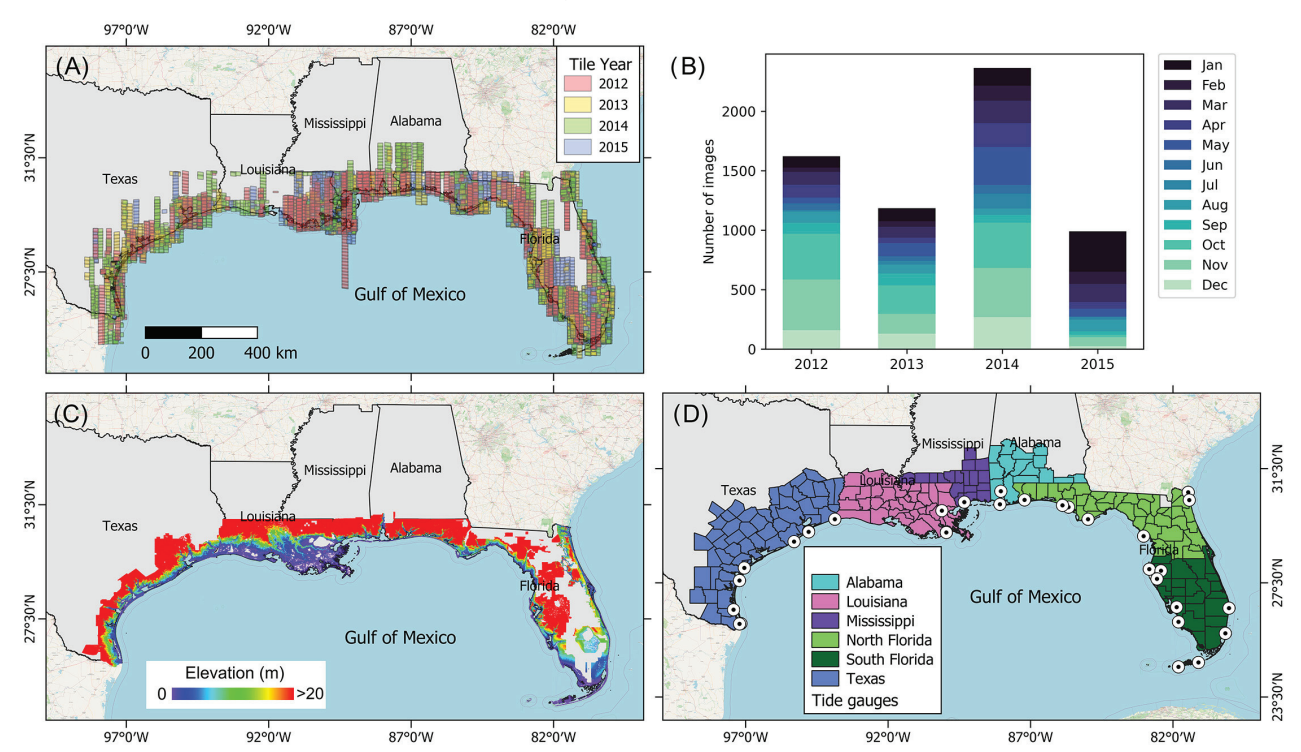


Figure 1. Map of the study area. **(A)** Spatial and **(B)** temporal distribution and coverage of the WorldView-2 and WorldView-3 tiles used. **(C)** Coverage of the airborne Lidar-derived digital elevation model DEM (2 m horizontal resolution). **(D)** Counties per state covered in this study (North Florida and South Florida counties were separated by county boundaries at 28.2°N, approximately). Location of tide gauges used to derive sea level rise trends are shown as white circles with a black center.

Table 1. WorldView-2 and WorldView-3 multispectral sensor specifications.

| Band Name | Band Number | Center Wavelength (nm) | Band Coverage (nm) | Effective Bandwidth (nm) |
|-------------|-------------|------------------------|--------------------|-----------------------------|
| WorldView-2 | | | | |
| Coastal | 1 | 427 | 396-458 | 47 |
| Blue | 2 | 479 | 442-515 | 54 |
| Green | 3 | 546 | 506-586 | 63 |
| Yellow | 4 | 608 | 584-632 | 37 |
| Red | 5 | 659 | 624-694 | 57 |
| Red edge | 6 | 724 | 699-749 | 39 |
| NIR I | 7 | 833 | 765-901 | 99 |
| NIR II | 8 | 950 | 856-1043 | 100 |
| WorldView-3 | | | | |
| Coastal | 1 | 426 | 397-454 | 41 |
| Blue | 2 | 481 | 445-517 | 54 |
| Green | 3 | 547 | 507-586 | 62 |
| Yellow | 4 | 605 | 580-629 | 38 |
| Red | 5 | 661 | 626-696 | 59 |
| Red edge | 6 | 724 | 698-749 | 39 |
| NIR I | 7 | 832 | 765-899 | 100 |
| NIR II | 8 | 948 | 857–1039 | 89 |

Remote Sens. 2024, 16, 2052 4 of 17

2.3. Land Cover Classification

Images were prepared for the land cover classification following McCarthy et al. [11]. This included file ingestion, orthorectification, re-gridding and mapping, radiometric calibration, atmospheric correction, and generation of remote sensing reflectance (Rrs). Radiometric calibration was performed by applying factors provided by Maxar. The atmospheric correction accounted for Rayleigh scattering. Then, Rayleigh-scattered radiances were converted to Rrs. The pre-processing steps were performed using the Central Instructional and Research Computing Environment (CIRCE) cluster computer at the University of South Florida.

A decision tree developed and tested by McCarthy et al. [11] in West Florida was used for land cover classification, using the spectral bands shown in Table 1. Ten output classes included: clouds, soil, water, dead grass, marsh, scrub, grass, forested upland, forested wetland, and developed land. Pixel values for the classes were from 1 to 10, respectively for each class. Pixels with no data were assigned a value of 0. This included pixels identified as clouds and shadows. The decision nodes used multiple spectral indices and thresholds to make pixel classifications (Figure A1).

We generated a composite land cover map for the whole study area representing January 2012 through December 2015 (inclusive) by stacking classified land cover images and retaining only the maximum classification values pixel-by-pixel (i.e., where pixels from two or more mapped images overlapped, the higher of the classification values was retained). As an example, all classes by definition have a value greater than "clouds" (class value equal to 0), so a "cloud" pixel would always be ignored in favor of a higher-valued class in the final mosaic. This method introduces a potential bias towards higher-valued classes in areas covered by many images compared to areas covered by few images.

The composite map was developed using all useful data between 2012 and 2015. Differences in vegetation at each pixel within this three-year period were considered negligible. We found that differences in vegetation were less than 0.8% per state relative to land cover data between 2013 and 2016 from the NLCD product (Table A1). These changes in vegetation were estimated for a coastal elevation band between 0 and 10 m above mean sea level (see Section 2.6). In specific images, bare land, water, and developed classes were often confused and misclassified in the 2012–2015 mosaic. We recomputed the mosaic for specific areas where misclassifications were observed. In those cases, we prioritized the most probable classes that may occupy that area (e.g., water pixels were priority near inland water bodies and coastal areas; developed pixels were priority in urban areas). We used the 2018 Topologically Integrated Geographic Encoding and Referencing (TIGER) data set from the U.S. Census Bureau to clip the landcover mosaic. We used images covering areas out to the three-mile territorial sea limit along the shoreline. As a consequence, the "water area" estimated from our classification approach is a total measurement including inland, coastal, and three miles of territorial sea. This has no consequence for the study results, which focused on terrestrial land cover classes. The intermediate and final products were included in what we refer to here as the 3D-Wetlands land cover map.

While the classifications used no ground data for training or validation in other areas outside Florida, the composite map from 2012 to 2015 was validated using the USGS NLCD 2016 product, available in GEE. The NLCD is a 30 m resolution Landsat-based product spanning 8 years: 2001, 2004, 2008, 2011, 2013, 2016, 2019, and 2021. It provided rigorously validated land cover data for 20 classes [14]. The NLCD is the best reference available for land cover types along the US Gulf of Mexico coast. We focused validation on total vegetated areas and wetlands only (our "forested wetlands" would be equivalent to "woody wetlands" in the NLCD). We merged some vegetation classes as described in Table A2 to minimize uncertainties around individual classes. To conduct the validation using NLCD, we generated 1000 random points per state in our vegetated classes located in the 0–10 m topographic elevation band (see Section 2.6). The number of usable points varied due masking of pixels with no data or other causes that led to invalid classes. As result, we identified 835 points in Alabama, 894 in Louisiana, 789 in Mississippi, 848 in Texas, 863 in

Remote Sens. 2024, 16, 2052 5 of 17

North Florida, and 641 in South Florida for validation against the NLCD. The locations of those points were sampled over the NLCD 2016 product. We generated error matrices, and the overall accuracy, user's and producer's accuracies were estimated [22]. Validation results against the NLCD 2016 product showed that the total vegetation classes were 100% accurate (in overall accuracy, and user's and producer's accuracies) in all regions within the 10 m elevation band. The validation for wetlands areas showed variable accuracies (Table A3). Overall accuracies ranged from 47% to 85%, while the producer's accuracy from 37% to 72%, and user's accuracy from 37% to 83%.

2.4. Digital Elevation Model Data

The topographic model to match the landcover classification used 197 Lidar data sets totaling 6.1 TB of point clouds arranged in 193,573 tiles with acquisition dates from 1998 to 2018 (Table 2). From the original tiles, we generated 281 bare-earth tiles of 40 km by 40 km covering the coastal regions of the 5 U.S. Gulf of Mexico states (Table A4). The final 2 m by 2 m bare-earth Digital Elevation Model (DEM) products totaled 432 GB. The DEM data set covers approximately 168,135 km² of the study area (Figure 1C).

Table 2. The Lidar data used for the 3D-Wetlands product.

| State | UTM Zones | Data Sets | Volume (TB) | Tiles | Years |
|-------------------------|-----------|-----------|-------------|---------|--------------|
| Texas | 14, 15 | 37 | 1.69 | 37,594 | 2005 to 2018 |
| Louisiana | 15, 16 | 20 | 0.52 | 23,657 | 2002 to 2017 |
| Mississippi and Alabama | 16 | 30 | 0.72 | 24,303 | 1998 to 2018 |
| Florida | 16, 17 | 110 | 3.17 | 108,020 | 2001 to 2018 |
| Total | | 197 | 6.10 | 193,573 | |

Lidar data were originally acquired by various entities working to meet different product specifications and using different survey parameters, instruments, software, and procedures. This resulted in varying quality of the Lidar point data. We took a priority weighted averaging approach to join multiple Lidar data sets in areas where there was overlap between surveys to achieve the optimum topographic model to match with World-View imagery. Thus, the 2 m surfaces were the integrated results of changes in Lidar survey technology, human construction, and natural changes including ground subsidence during the 20-year period sampled. The processing workflow occurred in six phases, as follows:

- 1. Checked metadata of each Lidar survey data set for (1) horizontal and vertical datums, (2) horizontal coordinate system, (3) horizontal unit, (4) elevation unit, (5) geoid used, and (6) nominal point interval.
- 2. Reviewed when and by whom the survey was conducted, and the accuracy provided in the metadata to help in setting the priority of each data set. Data sets with higher accuracy, denser point clouds, and newer acquisition dates had higher priority.
- 3. Converted all Lidar tiles into point clouds having the NAD83 horizontal datum, UTM horizontal coordinate system in meters, NAVD88 vertical datum with vertical coordinate in meters, and the use of Geoid2012b for transformation to NAVD88.
- 4. Generated 2 m pixel elevation surfaces (bare-earth and all-point) on each Lidar tile using an inverse distance weighting algorithm that searches for the 3 nearest points within a 3 m radius of the pixel. Bare-earth and all-points point density per 2 m pixel also were generated for each Lidar tile.
- 5. Mosaicked all elevation surface tiles for each Lidar data set into raster files of 20,000 by 20,000 pixels (40 km by 40 km). Identified data gaps in the raster files using morphological filters and fill gaps by interpolating from neighboring pixels.
- 6. Generated final elevation surfaces by overlapping the mosaicked raster files of these Lidar data sets with priority weighted averaging. In addition, a 10-pixel buffer was used to smooth the surface along edges of Lidar data sets. The final data products were raster files of 20,000 by 20,000 (40 km by 40 km) 2 m pixels covering each UTM zone in each state.

Remote Sens. **2024**, 16, 2052 6 of 17

2.5. Sea-Level Trends

Time series of sea level data from 31 tide gauge stations spanning our study area were downloaded from NOAA (https://tidesandcurrents.noaa.gov/sltrends/; accessed on 3 June 2024) (Figure 1D). The seasonal cycle in these data had already been removed by the provider. The coordinates and sea-level trends of each tide gauge station are shown in Table A5.

We used data from the period 1983–2021 across the stations to avoid large data gaps that are pervasive in earlier data. To derive trends in sea level, all tide gauge data in each state or in subregions of a state were averaged over a year, and linear sea-level trends (mm yr⁻¹) obtained. The trends were used to project sea level scenarios for the years 2030, 2050, 2070, and 2100, using 2015 as a baseline. SLR was assumed to be linear over the period of the extrapolation; this ignored any possible change in factors that might influence sea level, such as seawater warming rate, hydrological imbalances, land subsidence, and land development rates. Confidence intervals of 90% were calculated as one standard error multiplied by 1.65. The state of Florida was divided into North Florida and South Florida at a latitude of 28.2°N (Figure 1D), to facilitate the analysis and reduce bias due to different sea-level trends (Table A5). Linear trends and confidence intervals were estimated using Scilab v6.1.1.

2.6. Analytical Approach

We used GEE to store 10,245 classified images (2009–2018), create mosaics, and quantify areas. All the classified images and DEMs are publicly available through a GEE App that allows creation of user-defined mosaics, overlay and comparison with topography, aggregation of products at the level of individual counties, and comparing change in land cover over time (https://lizcanosandoval.users.earthengine.app/view/hr-land-cover-gulf-of-mexico; accessed on 3 June 2024).

To analyze change in land cover extent in future sea-level rise scenarios, we estimated the surface area covered by each land cover class in each state by multiplying the area of a single pixel $(2 \text{ m} \times 2 \text{ m})$ by the number of pixels in a class, as clipped given different future sea level states. The region between the sea and the 10 m coastal elevation is of interest because of potential flood and erosion risk and therefore is a focus for coastal area management. Sea level scenarios projected for 2030, 2050, 2070, and 2100 were used to estimate potential reductions in total surface area for each coastal vegetation class in cumulative elevation bins across the different states, relative to the land cover product for the period 2012–2015.

Sea level projections were made at 0.1 m scale to match the vertical DEM resolution. We focused on relative changes in the total mapped area and the area occupied by five specific vegetation classes: marsh, scrub, grass, forested upland, and forested wetland. We considered marshes and forested wetlands as the principal coastal wetland classes. Total land area estimations excluded pixels classified as no data, cloud, and water. Therefore, any estimates in area extent for any class may be considered conservative.

Comparisons between land cover profiles from our 3D-Wetlands product and the USGS NLCD from 2016 focused on total vegetation and wetlands and they were considered as validation of land cover profiles. Only the NLCD product congruent with the 3D-Wetlands mosaic was used in the comparison. Area estimations were made using the native pixel resolution of each product along the 0–10 m elevation profile at 0.1 m intervals. Pearson's correlations were made for each comparison between total vegetation and wetlands per state. The area comparisons per elevation ranges can be seen in Figure A2. The correlations of total vegetation between the two products were r > 0.93 in each state, but the wetland areas were more variable being low in North Florida (r = 0.12) and Alabama (r = 0.51), and mid to high in the other states (r > 0.73). Correlation coefficients are shown in Figure A2.

All data were visualized using the Seaborn package in Python and mapped using QGIS v3.18 and the GEE plugin.

Remote Sens. **2024**, 16, 2052 7 of 17

3. Results

3.1. Mapped Area

The total area mapped for the period 2012–2015 between the coast and 10 m elevation above sea level in the US Gulf of Mexico was 293,718 km². Of this, we mapped 23,432 km² in Alabama, 52,959 km² in Louisiana, 13,206 km² in Mississippi, 63,602 km² in North Florida, 67,887 km² in South Florida, and 72,632 km² in Texas (this excludes no data and cloudy pixels in the final composite) (Figure 2). Louisiana had the least area covered by satellite imagery (Figures 2 and 3). The total "no data" area in the 10 m elevation coastal band, including cloudy pixels, represented 39.9 km² (3.1%) in Alabama, 12,213 km² (35.2%) in Louisiana, 6.5 km² (0.3%) in Mississippi, 3,873 km² (20.8%) in North Florida, 2224 km² (9.2%) in South Florida, and 1222 km² (5.1%) in Texas. In total, 18.6% of the 10 m elevation band across the entire study region was missing data. We therefore chose to examine abundance of wetland land cover classes relative to overall vegetated land cover classes for each state.

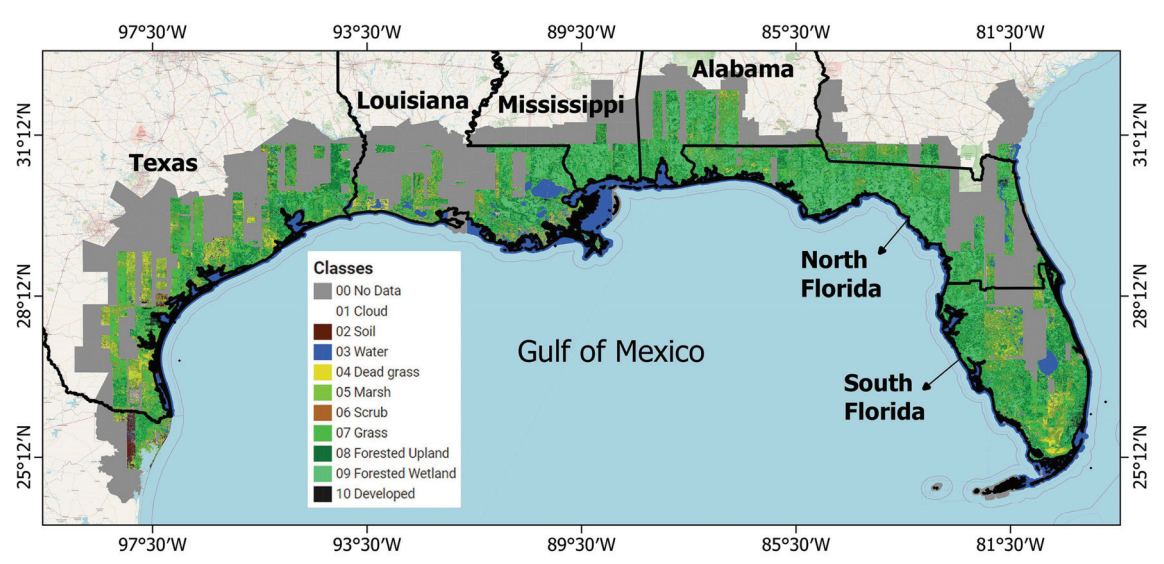


Figure 2. 3D-Wetland land cover map at 2 m resolution of the south and southeast US coast for period 2012–2015. The mosaic shape is bounded at a county level.

3.2. Vegetation and Wetland Extent within 0-10 m Elevation from the Coast

Within the 10 m coastal vertical profiles of land cover per state composited between 2012 and 2015 (Figure 3), vegetated areas represented between 72.1% and 90.4% of the land area across the different regions (Table 3). Coastal wetlands area in relation to the total vegetation area for each state represented 35.6% in Alabama, 24.4% in Louisiana, 39.5% in Mississippi, 46.3% in North Florida, 30.4% in South Florida, and 12.1% in Texas. Total coastal wetland area was 17,746.7 km 2 , of which 60.9% was observed in Florida.

Together, Florida and Louisiana represented 72.5% of the total vegetated areas examined. Forested wetlands were the dominant vegetation type in Alabama, Mississippi, and North Florida. The dominant vegetated classes in Louisiana, Texas, and South Florida were grass and forested upland.

3.3. Mean Sea-Level Trends

The mean sea-level trends computed for the period 1983–2021 show that Louisiana had the fastest SLR rate, with 7.96 mm \pm 1.36 mm yr $^{-1}$. South Florida and North Florida showed the slowest SLR rates at 4.19 mm \pm 0.60 mm yr $^{-1}$ and 4.02 mm \pm 0.71 mm yr $^{-1}$, respectively (Figure 4A). Sea-level projections showed Louisiana will experience an increase of 0.68 m \pm 0.12 m by 2100 relative to 2015 (Figure 4B). The overall sea-level increases by 2100 are 0.51 m \pm 0.08 m for Texas, 0.43 m \pm 0.07 m for Alabama, 0.40 m \pm 0.06 m for

Remote Sens. **2024**, 16, 2052 8 of 17

Mississippi, 0.36 m \pm 0.05 m for South Florida, and 0.34 m \pm 0.06 m for North Florida. These rates may now be considered conservative as sea-level rise in the region accelerated in the last decade (i.e., 2010–2021), exceeding 10 mm yr⁻¹ in some areas [23].

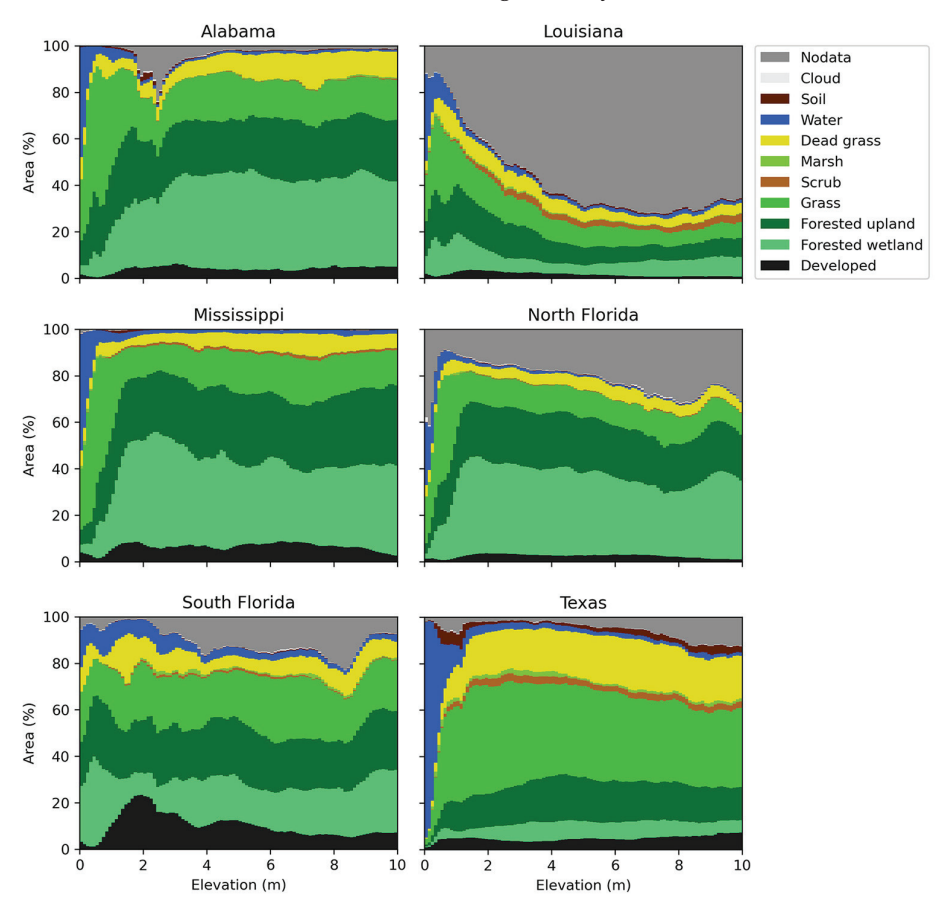


Figure 3. Land cover area (%) along the southeast U.S. coast along the 0-10 m elevation band.

Table 3. Vegetation and total land area (km²) of the 0–10 m elevation band along the coast of the southeastern United States. Total land area does not include water pixels. Missing data included non-valid pixels and cloud pixels.

| Classes | Alabama | Louisiana | Mississippi | North Florida | South Florida | Texas |
|----------------------------|----------------|---|---------------|--------------------|--------------------|--------------------|
| Marsh | 2.9 | 337.1 | 5.5 | 31.1 | 192.1 | 355.6 |
| Scrub | 2.3 | 470.9 | 19.2 | 45.8 | 151.2 | 570.3 |
| Grass | 364.8 | 6889.6 | 493.5 | 2879.6 | 5282.2 | 8603.5 |
| Forested upland | 316.6 | 5302.0 | 598.2 | 4002.6 | 5589.2 | 3471.3 |
| Forested wetland | 375.6 | 3758.5 | 720.0 | 5950.6 | 4626.9 | 1390.6 |
| Total Vegetation | 1062.2 | 16,758.1 | 1836.3 | 12,909.8 | 15,841.6 | 14,391.3 |
| Total Land Missing Data | 1217.9 39.9 | 19,724.5 12,213.0 | 2104.5 6.5 | 14,280.2 3872.6 | 20,572.8 2223.7 | 19,952.1 1221.6 |
| 0 | | , | | | | |

3.4. Projected Area Loss with SLR

All states show progressive losses in total area with time, and some states will see higher losses due to their topography (Figure 5). The projected losses in total land and vegetation areas due to sea-level rise are largest in Louisiana, due to the highest sea-level rise trend and the large area of low-lying lands. Louisiana is projected to experience a loss of approximately 11,351 km² to be covered by water in 2100. Of this, 88.8% is vegetated area and 11.2% is occupied by other land cover classes (Table 4). This is followed by Florida and Texas as these two states have much larger low-lying coastal vegetated areas than Mississippi or Alabama (Figure 5). Alabama and Mississippi are expected to have relatively

Remote Sens. 2024, 16, 2052 9 of 17

small coastal land area losses (<80 km²) because they have shorter coastlines and more elevated topography.

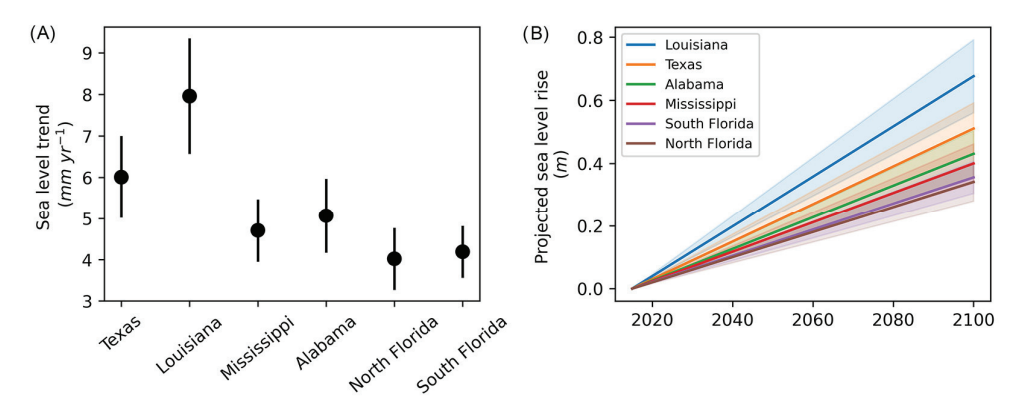


Figure 4. (**A**) Mean sea-level trends and confidence intervals at 90% for period 1983–2021 for the southeastern U.S. (**B**) Projections of sea level rise from 2015 to 2100 for each region with 90% confidence intervals.

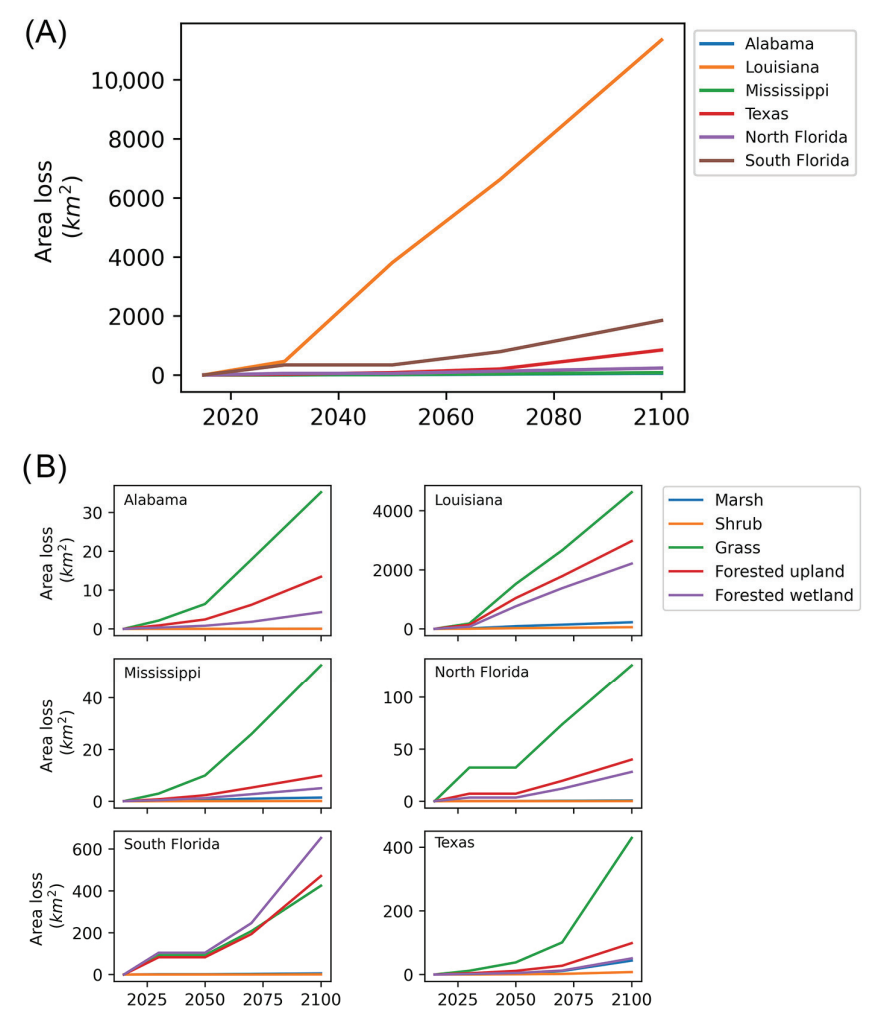


Figure 5. Projected losses in total land (**A**) and vegetation (**B**) areas by future sea-level rise. Marsh and forested wetland are considered as coastal wetlands in this study.

Table 4. Estimated losses in area (km²) due to sea-level rise by 2100 in the southeastern U.S. Marsh and forested wetland are considered as coastal wetlands in this study. The total land area includes total vegetation and other classes such as soil, dead grass, and developed.

| Classes | Alabama | Louisiana | Mississippi | North Florida | South Florida | Texas | Total |
|------------------|---------|-----------|-------------|---------------|---------------|--------|----------|
| Marsh | < 0.1 | 222.9 | 1.4 | 0.6 | 5.4 | 43.7 | 273.9 |
| Scrub | < 0.1 | 56.2 | < 0.1 | 0.1 | 0.5 | 7.7 | 64.6 |
| Grass | 35.2 | 4623.4 | 52.7 | 130.8 | 424.4 | 429.1 | 5695.6 |
| Forested upland | 13.4 | 2971.0 | 9.8 | 39.8 | 470.7 | 98.5 | 3603.3 |
| Forested wetland | 4.3 | 2209.1 | 5.0 | 28.1 | 652.7 | 50.7 | 2949.8 |
| Vegetation | 52.9 | 10,082.6 | 68.9 | 199.4 | 1553.8 | 629.7 | 12,587.2 |
| Land | 57.9 | 11,350.9 | 78.2 | 233.7 | 1846.2 | 844.7 | 14,411.7 |
| Water | 15.2 | 2283.7 | 33.0 | 115.2 | 243.5 | 2051.3 | 4742.0 |
| No Data | 0.1 | 2019.1 | 1.2 | 208.8 | 82.0 | 69.8 | 2381.0 |

In 2100, the area of coastal wetlands (forested wetlands and marshes) at risk of flooding due to SLR is estimated to be at least $2432 \, \mathrm{km^2}$ in Louisiana, $6.4 \, \mathrm{km^2}$ in Mississippi, $94.4 \, \mathrm{km^2}$ in Texas, $28.6 \, \mathrm{km^2}$ in North Florida, and $658 \, \mathrm{km^2}$ in South Florida. The largest gaps in imagery coverage for areas projected to be affected by SLR in 2100 were observed in North Florida (37.4%) and Louisiana (12.9%) (Table 4). Other regions exhibited minor data gaps of <4% (Figure 3). However, even considering these gaps, at least $14,412 \, \mathrm{km^2}$ of land are at risk by 2100 in the southeast U.S. coast, of which $12,587 \, \mathrm{km^2}$ are vegetated areas. Of these areas, $3224 \, \mathrm{km^2}$ comprise wetlands, defined by forested wetlands and marshes.

4. Discussion

The advent of high-speed computing and high-resolution satellite images allows for fast processing of large amounts of data with unprecedented resolution at scale [11]. Still, satellite data often lacks uniform coverage of desired areas over time. Cloud-free coverage of the south and southeast US in the WorldView satellite data catalog is spotty in space and in time. We focused on the 2012 to 2015 period to create a land cover mosaic with only 18.6% data gaps in the 0–10 m elevation band along the coast for this region. The seasonal distribution of images also introduced other artifacts in the land cover mosaic that we did not quantify, including seasonal vegetation changes (phenology), changing water bodies including tides affecting cover in individual images, and changes in remote sensing reflectance simply due to differences in sensor–ground–sun view angles across time. Nevertheless, building composite mosaics of multiple images and retaining the vegetated classes led us to high accuracy assessments from which to project land cover losses due to SLR.

The mosaicking method prioritized vegetation and developed classes. We had misclassifications of the "developed" land class (built environment) because it was challenging to distinguish between developed land and some bare soil areas. These areas are often similar in brightness and confounded the classifier. These misclassifications were corrected manually in post-processing of the land cover products. The final 3D-Wetlands product was consistent with the Landsat-derived NLCD 2016 product. The NLCD 2016 product also has problems with land cover classification accuracies, such as confusion of water with wetlands, forest regrowth with permanent shrub/grasslands, and others, which were addressed in post-processing of the NLCD 2016 [14]. There were some differences between wetland classes of the 3D-Wetlands and NLCD 2016 that were likely due to pixel size differences, diversity in vegetation classes available in the NLCD 2016 product, and undetected misclassification errors, especially in Texas and Louisiana as indicated by the user's and producer's accuracies (Table A2). Spatial differences are large considering that one pixel of the NLCD at 30 m can contain 225 pixels of the 3D-Wetlands land cover at 2 m. The validation of the total vegetation showed a confidence of 100% that the 3D-Wetland was indicating vegetation correctly.

Florida and Louisiana are the states with most coastal area between the range of 0 and 10 m elevation, but the higher SLR trends along Louisiana's coast lead to the largest

Remote Sens. 2024, 16, 2052 11 of 17

projected vegetation loss in the region. At least 10,083 km² of Louisiana vegetation will likely be permanently inundated by 2100 relative to 2015. The gaps in our land cover data add some uncertainty by not knowing what land cover classes are represented at specific elevation ranges. Reed et al. [21] modeled three scenarios for Louisiana that corresponded to 0.43 m, 0.63 m, and 0.83 m of SLR between 2015 and 2064. They estimated land losses of 3005 km^2 , 5515 km^2 , and 9986 km^2 , respectively. Our estimates by 2070 (relative to 2015) with 0.44 m of SLR were at least 6620 km^2 of land loss.

In total, we estimated that more than 12,500 km² of vegetated land will be fully or near permanently covered by water in 2100 along the south and southeast U.S. coast. Different land cover, DEM data, and sea-level rise scenarios used by other studies on the U.S. and global coastal wetlands make it challenging to compare estimated wetland area losses (Table 5). Our study provided wetland extent and measured potential changes due to SLR at the finest available resolutions for the south and southeast coasts of the United States, and the SLR values we found for 2100 (0.3–0.7 m) fall among the mid-range projections (0.5–1.2 m, 90% probability) of a well-established probabilistic SLR model [24].

In this study, we assumed a linear SLR. Yet, global SLR accelerated at a rate of $3.1 \, \mathrm{mm} \, \mathrm{yr}^{-1}$ during 1993–2015, while areas along the northeast U.S. coast have shown accelerated rates as large as $6.1 \, \mathrm{mm} \, \mathrm{yr}^{-1}$ in the same period [25,26]. Dagendorf et al. [23] estimate even higher rates for the 2010–2021 period (>10 $\, \mathrm{mm} \, \mathrm{yr}^{-1}$). Some factors influencing SLR (other than deglaciation) at regional scales in the Gulf of Mexico and the U.S. east coasts are thermal expansion associated with the North Atlantic Oscillation and the El Niño-Southern Oscillation [26], river discharges [27], and land subsidence [28,29]. Along with water level changes, other perturbations may occur in coastal areas such as changes in salinity, water quality, and the overall landscape [20,30,31]. Potential vegetation and wetland losses due to SLR have been estimated and modeled under different future scenarios by other authors [18,19,21].

Table 5. Studies of coastal wetland changes due to sea-level rise (SLR) by 2100 in global and U.S. coasts.

| Measure | Study Area | Wetland Product | DEM Product | SLR Scenarios by 2100 | Reference |
|--|---|--|---------------------|--------------------------|-------------------------|
| Coastal wetland cover and change | Southeast U.S. | 3D-Wetlands (2 m) | Lidar (2 m) | 0.3–0.7 m | This study |
| Landward wetland migration | 39 estuaries in the Northern Gulf of Mexico coast | NWI (30 m) | Lidar (5, 10, 15 m) | 0.5, 1.0, and 1.5 m | Borchert et al. [32] |
| Coastal wetland change and potential refugia | U.S. Pacific and Atlantic coasts | Wetlands defined by tidal range and elevation data | NOAA Lidar (5 m) | 0.5–1.2 m and 0.9–2.4 m | Buchanan et al. [33] |
| Potential wetland loss and migration areas | U.S. Pacific and Atlantic coasts | C-CAP (30 m) | Not specified | 1.5–2.6 m | Osland et al. [20] |
| Coastal wetland change | Global coast | UNEP WCMC Databases | NASA STRM (90 m) | 2.9, 5.0, and 1.1 m | Schuerch et al. [19] |
| Coastal wetland change | Global coast | GLWD-3 (1 km) | NASA STRM (90 m) | 1 m | Blankespoor et al. [18] |

Resilience of wetlands to SLR and their capacity to migrate will depend on availability of accommodation space, which is influenced by sediment deposition rates, coastal human population, and infrastructures [19,20,32–35]. This might cause losses in aboveground carbon in the future due to potential transitions from forests to marshes [36]. However, recent findings on the organic production (vertical accretion) of coastal wetlands suggests that these ecosystems might keep the pace with SLR. Morris and Sundberg [37] found in monitoring sites at North Inlet estuary, South Carolina that marshes had higher rates of positive elevation (4.7 mm $\rm yr^{-1}$) than the local rate of SLR (3.4 mm $\rm yr^{-1}$) due to organic

Remote Sens. 2024, 16, 2052 12 of 17

production, suggesting a possible stability of the ecosystem for more than a century. Similar findings by Weston et al. [38] along the US East coast suggest accelerated marsh accretion in response to SLR. Tidal regimes also play a role in wetland accretion rates. Belliard et al. [39] found that several global coastal wetland sites with semi-diurnal tides show positive elevation changes relative to local SLR, in contrast to other tidal regimes such as diurnal and mixed-diurnal, where elevation deficits were observed.

If wetland refugia are conserved (with no human development) under optimistic scenarios (high positive surface elevation change rate of 8 to >10 mm yr $^{-1}$ and low greenhouse gas emissions), wetlands may increase by 25% in the United States, except for Louisiana [33]. Conservation and restoration strategies will be costly. The state of Louisiana already invested nearly USD 300 million in wetland restoration between 2012 and 2017 [40], and planned diversions of the Mississippi River are caught in contentious political discussions that risk accelerated land losses if not resolved. Overall, potential wetland drowning may represent losses of upwards of USD 732 billion in annual ecosystem services by 2100 in the United States [33].

5. Conclusions

The 3D-Wetlands land cover product demonstrated high accuracy in indicating vegetation, highlighting its reliability for further analysis in wetland areas. High-resolution land cover and topography products will enable more accurate estimations and potential studies on coastal wetlands. Regional differences in vegetation losses due to SLR are more critical in lowland areas such as Louisiana, which is expected to suffer the largest losses in vegetation area by 2100, including a large portion of coastal wetlands across the Northern Gulf of Mexico coast. This vulnerability underscores the importance of understanding coastal wetland extent and distribution for effective management, conservation, and planning.

Author Contributions: Conceptualization, L.L.-S., F.E.M.-K. and J.G.; methodology, L.L.-S., F.E.M.-K., M.J.M., T.M., D.R.-R. and J.G.; software, L.L.-S., T.M. and D.R.-R.; validation, L.L.-S., M.J.M. and T.M.; formal analysis, L.L.-S.; investigation, L.L.-S.; resources, L.L.-S.; data curation, L.L.-S.; writing—original draft preparation, L.L.-S. and J.G.; writing—review and editing, L.L.-S., J.G., M.J.M., T.M., D.R.-R. and F.E.M.-K.; visualization, L.L.-S.; supervision, F.E.M.-K.; project administration, F.E.M.-K.; funding acquisition, F.E.M.-K. and J.G. All authors have read and agreed to the published version of the manuscript.

Funding: This work was supported by the NSF (grant 1762493: Spokes: MEDIUM: SOUTH: Collaborative: Enhanced 3-D Mapping for Habitat, Biodiversity, and Flood Hazard Assessments of Coastal and Wetland Areas of the Southern US), by the Marine Biodiversity Observation Network (MBON: NASA grants NNX14AP62A; 80NSSC20K0017; 80NSSC22K1779; NOAA IOOS grant NA19NOS0120199), and the Gulf of Mexico Coastal Ocean Observing System (GCOOS/IOOS Cooperative Agreement NA16NOS0120018).

Data Availability Statement: The 3D-Wetland products (land cover and DEM data) are available at the interactive Google Earth Engine App at country scale: https://lizcanosandoval.users.earthengine.app/view/hr-land-cover-gulf-of-mexico (accessed on 3 June 2024). Documentation from the 3D-Wetland products is available at: https://github.com/luislizcano/3D-wetlands-app (accessed on 3 June 2024). Tide gauge data were downloaded from NOAA at: https://tidesandcurrents.noaa.gov/sltrends/ (accessed on 3 June 2024). The land cover and DEM mosaic of the entire US Gulf of Mexico presented here, and codes are available upon request to the authors. Raw satellite imagery from WorldView is property of DigitalGlobe (© 2023 Maxar, USG Plus).

Acknowledgments: We thank the University of South Florida for the support and use of the cluster computer (CIRCE) for processing and reprocessing of thousands of satellite images. We thank Sebastian DiGeronimo for his help in satellite imagery acquisition and land cover classification. Special thanks to the Fulbright Program of Colombia, Colciencias, College of Marine Science at USF, and NASA for supporting the doctoral studies and research of L. Lizcano-Sandoval with the Fulbright-Colciencias Scholarship, Norman Blake Endowed Memorial Fellowship, and Sanibel-Captiva Shell Club/Mary & Al Bridell Memorial Fellowship, and NASA FINESST.

Conflicts of Interest: The authors declare no conflicts of interest.

Appendix A

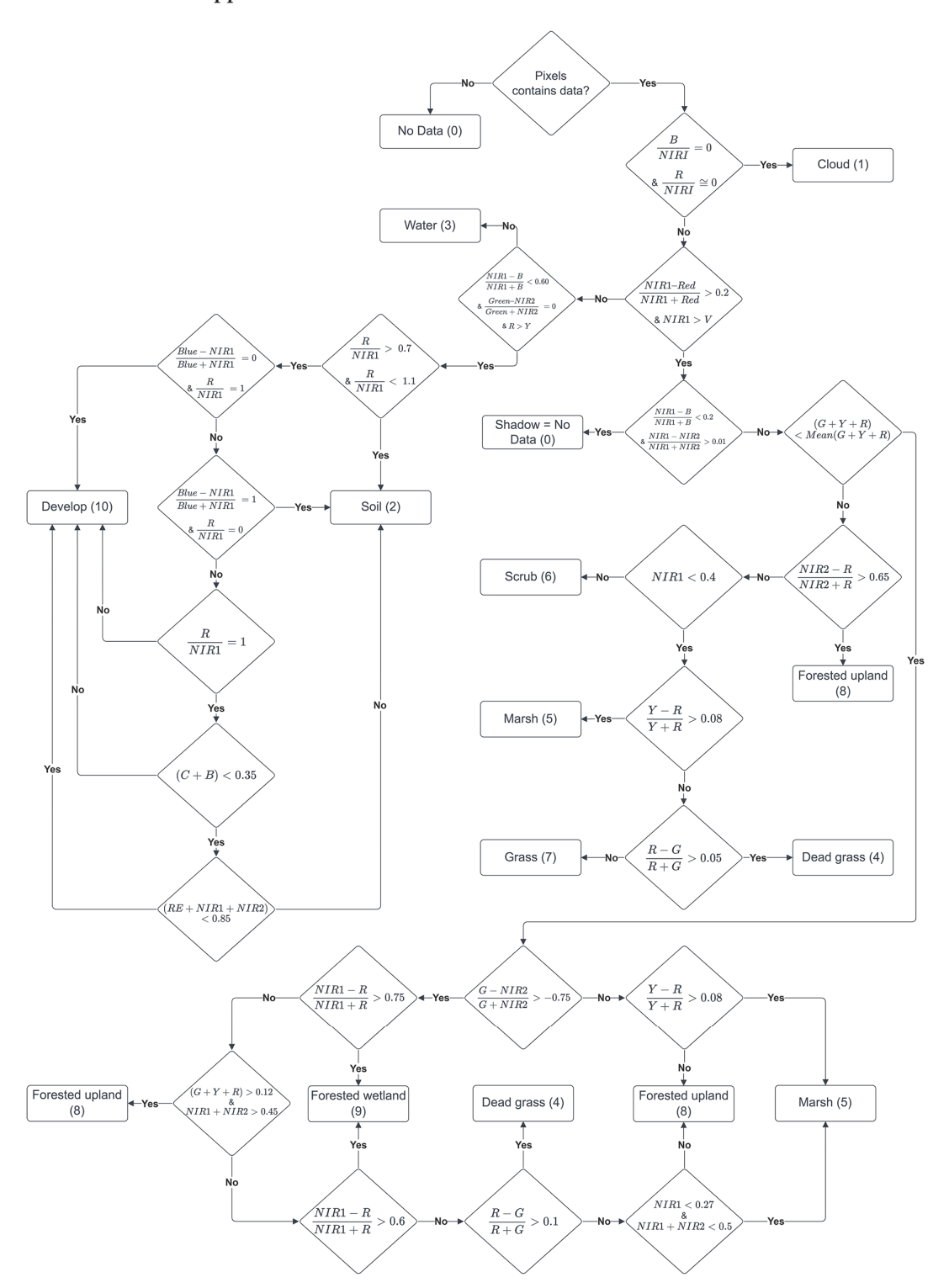


Figure A1. Decision tree classifier for land cover with ten classes. Number in parenthesis in each class box represent the pixel class. WorldView-2 and WorldView-3 bands used are C: coastal; B: blue; G: green; Y: yellow; R: red; RE: red edge; NIR1: near-infrared I; and NIR2: near-infrared II.

Appendix B

Table A1. Changes (%) in vegetation areas (km²) between the NLCD 2013 and NLCD 2016 products along an elevation band of 0–10 m of different coasts of the southeastern U.S.

| Coast | 2013 (km ²) | 2016 (km ²) | Change (%) |
|---------------|-------------------------|-------------------------|------------|
| Texas | 18,094 | 18,235 | 0.78 |
| Mississippi | 1623 | 1620 | -0.16 |
| Louisiana | 30,520 | 30,408 | -0.37 |
| Alabama | 1027 | 1026 | -0.05 |
| North Florida | 14,760 | 14,730 | -0.20 |
| South Florida | 16,106 | 16,063 | -0.27 |

Appendix C

Table A2. Classes representing the total vegetation from our project 3D-Wetlands and the NLCD product. The classes "forested wetland" (3D-Wetlands) and "woody wetlands" (NLCD) were the only ones similar enough conceptually for a direct comparison.

| 3D-Wetlands | NLCD |
|------------------|-------------------|
| Marsh | Deciduous forest |
| Scrub | Evergreen forest |
| Grass | Mixed forest |
| Forested upland | Shrub/Scrub |
| Forested wetland | Grassland |
| | Pasture |
| | Cultivated crops |
| | Woody wetlands |
| | Emergent wetlands |

Appendix D

Table A3. Overall accuracy (OA) and producer's (PA) and user's (UA) accuracies of the wetland class validation per state. Accuracies presented in percentages.

| State | PA | UA | OA |
|---------------|------|------|------|
| Alabama | 37.1 | 68.5 | 47.3 |
| Louisiana | 42.9 | 56.2 | 73.0 |
| Mississippi | 56.5 | 72.8 | 60.7 |
| Texas | 36.9 | 37.3 | 84.8 |
| North Florida | 72.4 | 59.3 | 61.1 |
| South Florida | 49.6 | 82.7 | 66.1 |

Appendix E

Table A4. The 2 m DEM generated by 40×40 km tile for the 3D wetlands product.

| State | UTM Zones | Bare-Earth Surface | | All-Point Surface | |
|-------------------------|--------------|--------------------|-------------|-------------------|-------------|
| oute | O I WI Zones | Tiles | Volume (GB) | Tiles | Volume (GB) |
| | 14 | 38 | 56.6 | 39 | 58.1 |
| Texas | 15 | 26 | 38.7 | 26 | 38.7 |
| т | 15 | 51 | 76.0 | 58 | 86.4 |
| Louisiana | 16 | 14 | 20.8 | 14 | 20.8 |
| Mississippi and Alabama | 16 | 19 | 28.3 | 19 | 28.3 |
| * * | 16 | 26 | 38.7 | 27 | 40.2 |
| Florida | 17 | 107 | 159.5 | 107 | 159.5 |
| Total | | 281 | 418.6 | 290 | 432 |

Appendix F

Table A5. Tide gauge stations along the US Gulf Coast and Florida. Sea-level rise (SLR) rates and 95% confidence intervals (CI) are also shown.

| State | Station Name | Longitude | Latitude | Begin | End | SLR Rate (mm/yr) | 95% CI (mm/yr) |
|-----------------|-------------------------|-----------|----------|-------|------|------------------|----------------|
| Alabama | Dauphin Island | -88.075 | 30.250 | 1966 | 2021 | 4.25 | 0.57 |
| Alabama | Mobile State Docks | -88.043 | 30.708 | 1980 | 2021 | 4.79 | 1.39 |
| Louisiana | Grand Isle | -89.957 | 29.263 | 1947 | 2021 | 9.18 | 0.38 |
| Louisiana | New Canal | -90.113 | 30.027 | 1982 | 2021 | 6.25 | 1.11 |
| Mississippi | Bay Waveland | -89.326 | 30.326 | 1978 | 2021 | 4.68 | 0.73 |
| Florida (North) | Fernandina Beach | -81.466 | 30.671 | 1897 | 2021 | 2.20 | 0.17 |
| Florida (North) | Mayport | -81.428 | 30.398 | 1928 | 2021 | 2.78 | 0.25 |
| Florida (North) | Cedar Key | -83.032 | 29.135 | 1914 | 2021 | 2.27 | 0.18 |
| Florida (North) | Apalachicola | -84.982 | 29.727 | 1967 | 2021 | 2.82 | 0.60 |
| Florida (North) | Panama City | -85.667 | 30.152 | 1973 | 2021 | 2.91 | 0.58 |
| Florida (North) | Panama City Beach | -85.879 | 30.214 | 1989 | 2021 | 4.90 | 0.95 |
| Florida (North) | Pensacola | -87.211 | 30.404 | 1923 | 2021 | 2.59 | 0.23 |
| Florida (South) | Lake Worth Pier | -80.034 | 26.613 | 1970 | 2021 | 3.82 | 0.51 |
| Florida (South) | Virginia Key | -80.162 | 25.731 | 1931 | 2021 | 3.00 | 0.21 |
| Florida (South) | Vaca Key | -81.106 | 24.711 | 1971 | 2021 | 3.95 | 0.42 |
| Florida (South) | Key West | -81.808 | 24.556 | 1913 | 2021 | 2.52 | 0.14 |
| Florida (South) | Naples | -81.807 | 26.132 | 1965 | 2021 | 3.21 | 0.43 |
| Florida (South) | Fort Myers | -81.871 | 26.648 | 1965 | 2021 | 3.37 | 0.44 |
| Florida (South) | St. Petersburg | -82.627 | 27.761 | 1947 | 2021 | 2.97 | 0.24 |
| Florida (South) | Clearwater Beach | -82.832 | 27.978 | 1973 | 2021 | 4.10 | 0.54 |
| Florida (South) | East Bay | -82.421 | 27.923 | 1976 | 2021 | 5.68 | 0.95 |
| Florida (South) | Port Manatee | -82.562 | 27.638 | 1976 | 2021 | 5.16 | 0.71 |
| Texas | Sabine Pass | -93.870 | 29.728 | 1958 | 2020 | 6.16 | 0.74 |
| Texas | Galveston Pier 21 | -94.793 | 29.310 | 1904 | 2021 | 6.62 | 0.22 |
| Texas | Galveston Pleasure Pier | -94.789 | 29.285 | 1957 | 2011 | 6.62 | 0.69 |
| Texas | Freeport | -95.302 | 28.943 | 1972 | 2020 | 4.21 | 0.72 |
| Texas | Rockport | -97.047 | 28.022 | 1937 | 2021 | 5.94 | 0.47 |
| Texas | Corpus Christi | -97.217 | 27.580 | 1983 | 2021 | 5.54 | 1.00 |
| Texas | Port Mansfield | -97.426 | 26.558 | 1963 | 2021 | 3.67 | 0.68 |
| Texas | South Padre Island | -97.168 | 26.073 | 1958 | 2021 | 4.27 | 0.54 |
| Texas | Port Isabel | -97.216 | 26.061 | 1944 | 2021 | 4.25 | 0.33 |

Appendix G

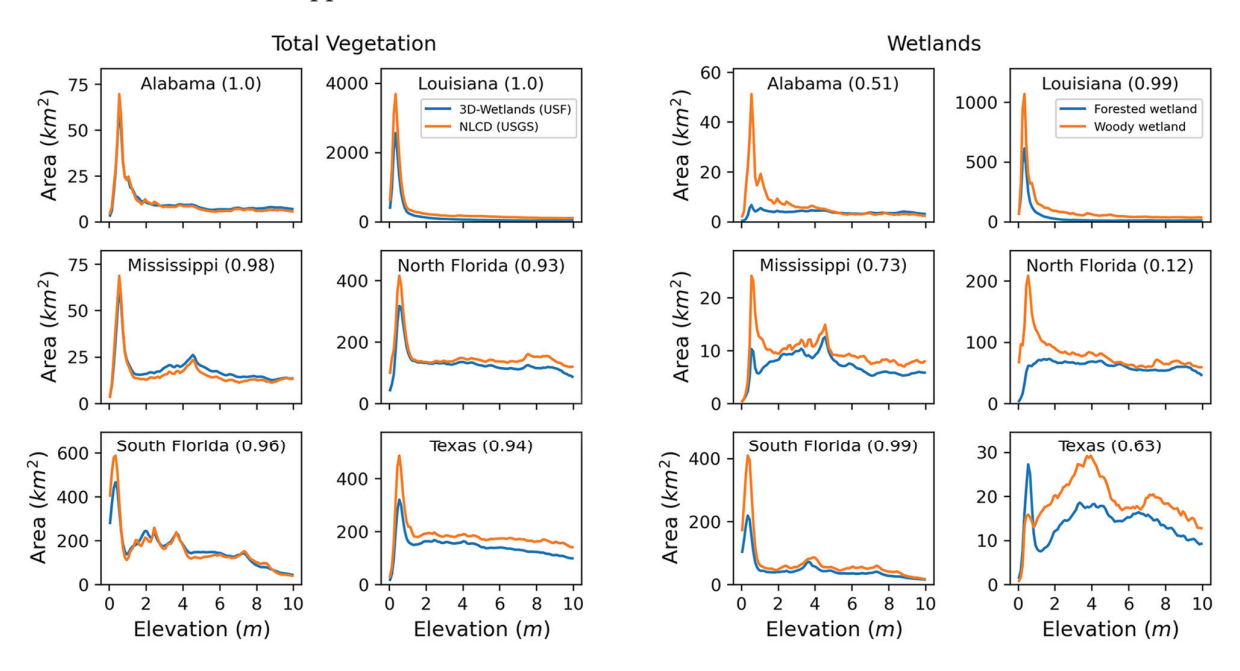


Figure A2. Comparison between the 3D-Wetlands (blue lines) and NLCD (orange lines) products per state. Pearson's correlation coefficients are shown in parenthesis, respectively. Left subplots represent comparisons of total vegetation. Right subplots represent comparisons of forested wetland classes.

References

1. Junk, W.J.; Brown, M.; Campbell, I.C.; Finlayson, M.; Gopal, B.; Ramberg, L.; Warner, B.G. The Comparative Biodiversity of Seven Globally Important Wetlands: A Synthesis. *Aquat. Sci.* **2006**, *68*, 400–414. [CrossRef]

- 2. Sheng, Y.P.; Rivera-Nieves, A.A.; Zou, R.; Paramygin, V.A. Role of Wetlands in Reducing Structural Loss Is Highly Dependent on Characteristics of Storms and Local Wetland and Structure Conditions. *Sci. Rep.* **2021**, *11*, 5237. [CrossRef] [PubMed]
- 3. Van Zelst, V.T.M.; Dijkstra, J.T.; van Wesenbeeck, B.K.; Eilander, D.; Morris, E.P.; Winsemius, H.C.; Ward, P.J.; de Vries, M.B. Cutting the Costs of Coastal Protection by Integrating Vegetation in Flood Defences. *Nat. Commun.* **2021**, *12*, 6533. [CrossRef] [PubMed]
- 4. Donato, D.C.; Kauffman, J.B.; Murdiyarso, D.; Kurnianto, S.; Stidham, M.; Kanninen, M. Mangroves among the Most Carbon-Rich Forests in the Tropics. *Nat. Geosci.* **2011**, *4*, 293–297. [CrossRef]
- 5. McLeod, E.; Chmura, G.L.; Bouillon, S.; Salm, R.; Björk, M.; Duarte, C.M.; Lovelock, C.E.; Schlesinger, W.H.; Silliman, B.R. A Blueprint for Blue Carbon: Toward an Improved Understanding of the Role of Vegetated Coastal Habitats in Sequestering CO₂. Front. Ecol. Environ. **2011**, *9*, 552–560. [CrossRef] [PubMed]
- Costanza, R.; de Groot, R.; Sutton, P.; van der Ploeg, S.; Anderson, S.J.; Kubiszewski, I.; Farber, S.; Turner, R.K. Changes in the Global Value of Ecosystem Services. Glob. Environ. Change 2014, 26, 152–158. [CrossRef]
- 7. Tiner, R.W. Wetland Indicators: A Guide to Wetland Identification, Delineation, Classification, and Mapping, 2nd ed.; Taylor & Francis: Boca Raton, FL, USA, 2017; ISBN 978-1-4398-5369-6.
- 8. Hu, S.; Niu, Z.; Chen, Y.; Li, L.; Zhang, H. Global Wetlands: Potential Distribution, Wetland Loss, and Status. *Sci. Total Environ.* **2017**, *586*, 319–327. [CrossRef] [PubMed]
- 9. Davidson, N.C.; Fluet-Chouinard, E.; Finlayson, C.M. Global Extent and Distribution of Wetlands: Trends and Issues. *Mar. Freshw. Res.* **2018**, *69*, 620. [CrossRef]
- 10. Mahdavi, S.; Salehi, B.; Granger, J.; Amani, M.; Brisco, B.; Huang, W. Remote Sensing for Wetland Classification: A Comprehensive Review. *GISci. Remote Sens.* **2018**, *55*, 623–658. [CrossRef]
- 11. McCarthy, M.J.; Radabaugh, K.R.; Moyer, R.P.; Muller-Karger, F.E. Enabling Efficient, Large-Scale High-Spatial Resolution Wetland Mapping Using Satellites. *Remote Sens. Environ.* **2018**, 208, 189–201. [CrossRef]
- 12. Wang, X.; Xiao, X.; Zou, Z.; Hou, L.; Qin, Y.; Dong, J.; Doughty, R.B.; Chen, B.; Zhang, X.; Chen, Y.; et al. Mapping Coastal Wetlands of China Using Time Series Landsat Images in 2018 and Google Earth Engine. *ISPRS J. Photogramm. Remote Sens.* 2020, 163, 312–326. [CrossRef] [PubMed]
- 13. Frazer, G.; Balis-Larsen, M.; Phinney, J.; Lang, M.; Bergeson, M. Technical Procedures for Conducting Status and Trends of the Nation's Wetlands (Version 2); U.S. Fish and Wildlife Service: Madison, WI, USA, 2017; p. 84.
- 14. Yang, L.; Jin, S.; Danielson, P.; Homer, C.; Gass, L.; Bender, S.M.; Case, A.; Costello, C.; Dewitz, J.; Fry, J.; et al. A New Generation of the United States National Land Cover Database: Requirements, Research Priorities, Design, and Implementation Strategies. *ISPRS J. Photogramm. Remote Sens.* **2018**, *146*, 108–123. [CrossRef]
- 15. Xu, T.; Weng, B.; Yan, D.; Wang, K.; Li, X.; Bi, W.; Li, M.; Cheng, X.; Liu, Y. Wetlands of International Importance: Status, Threats, and Future Protection. *Int. J. Environ. Res. Public Health* **2019**, *16*, 1818. [CrossRef] [PubMed]
- 16. Ramsar Convention on Wetlands. *Global Wetland Outlook: Special Edition 2021*; Secretariat of the Convention on Wetlands: Gland, Switzerland, 2021.
- 17. Fluet-Chouinard, E.; Stocker, B.D.; Zhang, Z.; Malhotra, A.; Melton, J.R.; Poulter, B.; Kaplan, J.O.; Goldewijk, K.K.; Siebert, S.; Minayeva, T.; et al. Extensive Global Wetland Loss over the Past Three Centuries. *Nature* 2023, 614, 281–286. [CrossRef] [PubMed]
- 18. Blankespoor, B.; Dasgupta, S.; Laplante, B. Sea-Level Rise and Coastal Wetlands. Ambio 2014, 43, 996–1005. [CrossRef] [PubMed]
- 19. Schuerch, M.; Spencer, T.; Temmerman, S.; Kirwan, M.L.; Wolff, C.; Lincke, D.; McOwen, C.J.; Pickering, M.D.; Reef, R.; Vafeidis, A.T.; et al. Future Response of Global Coastal Wetlands to Sea-Level Rise. *Nature* 2018, 561, 231–234. [CrossRef] [PubMed]
- 20. Osland, M.J.; Chivoiu, B.; Enwright, N.M.; Thorne, K.M.; Guntenspergen, G.R.; Grace, J.B.; Dale, L.L.; Brooks, W.; Herold, N.; Day, J.W.; et al. Migration and Transformation of Coastal Wetlands in Response to Rising Seas. *Sci. Adv.* **2022**, *8*, eabo5174. [CrossRef] [PubMed]
- 21. Reed, D.; Wang, Y.; Meselhe, E.; White, E. Modeling Wetland Transitions and Loss in Coastal Louisiana under Scenarios of Future Relative Sea-Level Rise. *Geomorphology* **2020**, *352*, 106991. [CrossRef]
- Congalton, R.G.; Green, K. Assessing the Accuracy of Remotely Sensed Data: Principles and Practices; CRC Press: Boca Raton, FL, USA, 2009; ISBN 978-1-4200-5512-2.
- 23. Dangendorf, S.; Hendricks, N.; Sun, Q.; Klinck, J.; Ezer, T.; Frederikse, T.; Calafat, F.M.; Wahl, T.; Törnqvist, T.E. Acceleration of U.S. Southeast and Gulf Coast Sea-Level Rise Amplified by Internal Climate Variability. *Nat. Commun.* 2023, 14, 1935. [CrossRef] [PubMed]
- 24. Kopp, R.E.; Horton, R.M.; Little, C.M.; Mitrovica, J.X.; Oppenheimer, M.; Rasmussen, D.J.; Strauss, B.H.; Tebaldi, C. Probabilistic 21st and 22nd Century Sea-level Projections at a Global Network of Tide-gauge Sites. *Earth's Future* 2014, 2, 383–406. [CrossRef]
- 25. Nicholls, R.J.; Cazenave, A. Sea-Level Rise and Its Impact on Coastal Zones. Science 2010, 328, 1517–1520. [CrossRef] [PubMed]
- 26. Domingues, R.; Goni, G.; Baringer, M.; Volkov, D. What Caused the Accelerated Sea Level Changes along the U.S. East Coast during 2010–2015? *Geophys. Res. Lett.* 2018, 45, 13367–13376. [CrossRef]

Remote Sens. 2024, 16, 2052 17 of 17

27. Piecuch, C.G.; Bittermann, K.; Kemp, A.C.; Ponte, R.M.; Little, C.M.; Engelhart, S.E.; Lentz, S.J. River-Discharge Effects on United States Atlantic and Gulf Coast Sea-Level Changes. *Proc. Natl. Acad. Sci. USA* 2018, 115, 7729–7734. [CrossRef]

- 28. Kuchar, J.; Milne, G.; Wolstencroft, M.; Love, R.; Tarasov, L.; Hijma, M. The Influence of Sediment Isostatic Adjustment on Sea Level Change and Land Motion along the U.S. Gulf Coast. *J. Geophys. Res. Solid Earth* **2018**, 123, 780–796. [CrossRef]
- 29. Piecuch, C.G.; Huybers, P.; Hay, C.C.; Kemp, A.C.; Little, C.M.; Mitrovica, J.X.; Ponte, R.M.; Tingley, M.P. Origin of Spatial Variation in US East Coast Sea-Level Trends during 1900–2017. *Nature* 2018, 564, 400–404. [CrossRef] [PubMed]
- 30. Dessu, S.B.; Price, R.M.; Troxler, T.G.; Kominoski, J.S. Effects of Sea-Level Rise and Freshwater Management on Long-Term Water Levels and Water Quality in the Florida Coastal Everglades. *J. Environ. Manag.* 2018, 211, 164–176. [CrossRef] [PubMed]
- 31. Meselhe, E.M.; White, E.D.; Wang, Y.; Reed, D.J. Uncertainty Analysis for Landscape Models Used for Coastal Planning. *Estuar. Coast. Shelf Sci.* **2021**, 256, 107371. [CrossRef]
- 32. Borchert, S.M.; Osland, M.J.; Enwright, N.M.; Griffith, K.T. Coastal Wetland Adaptation to Sea Level Rise: Quantifying Potential for Landward Migration and Coastal Squeeze. *J. Appl. Ecol.* **2018**, *55*, 2876–2887. [CrossRef]
- 33. Buchanan, M.; Kulp, S.; Strauss, B. Resilience of U.S. Coastal Wetlands to Accelerating Sea Level Rise. *Environ. Res. Commun.* **2022**, *4*, 61001. [CrossRef]
- 34. Cahoon, D.R.; McKee, K.L.; Morris, J.T. How Plants Influence Resilience of Salt Marsh and Mangrove Wetlands to Sea-Level Rise. *Estuaries Coasts* **2021**, *44*, 883–898. [CrossRef]
- 35. Ouyang, X.; Connolly, R.M.; Lee, S.Y. Revised Global Estimates of Resilience to Sea Level Rise for Tidal Marshes. *Environ. Chall.* **2022**, *9*, 100593. [CrossRef]
- 36. Smart, L.S.; Taillie, P.J.; Poulter, B.; Vukomanovic, J.; Singh, K.K.; Swenson, J.J.; Mitasova, H.; Smith, J.W.; Meentemeyer, R.K. Aboveground Carbon Loss Associated with the Spread of Ghost Forests as Sea Levels Rise. *Environ. Res. Lett.* **2020**, *15*, 104028. [CrossRef]
- 37. Morris, J.T.; Sundberg, K. Responses of Coastal Wetlands to Rising Sea-Level Revisited: The Importance of Organic Production. Estuaries Coasts 2024, 1–15. [CrossRef]
- 38. Weston, N.B.; Rodriguez, E.; Donnelly, B.; Solohin, E.; Jezycki, K.; Demberger, S.; Sutter, L.A.; Morris, J.T.; Neubauer, S.C.; Craft, C.B. Recent Acceleration of Wetland Accretion and Carbon Accumulation along the U.S. East Coast. *Earth's Future* 2023, 11, e2022EF003037. [CrossRef]
- 39. Belliard, J.; Gourgue, O.; Govers, G.; Kirwan, M.L.; Temmerman, S. Coastal Wetland Adaptability to Sea Level Rise: The Neglected Role of Semi-diurnal vs. Diurnal Tides. *Limnol. Ocean. Lett.* **2023**, *8*, 340–349. [CrossRef]
- 40. Coastal Protection & Restoration Authority of Louisiana. *Louisiana's Comprehensive Master Plan for a Sustainable Coast*; Office of Coastal Protection and Restoration: Baton Rouge, LA, USA, 2017; p. 171.

Disclaimer/Publisher's Note: The statements, opinions and data contained in all publications are solely those of the individual author(s) and contributor(s) and not of MDPI and/or the editor(s). MDPI and/or the editor(s) disclaim responsibility for any injury to people or property resulting from any ideas, methods, instructions or products referred to in the content.